

# OGLE-2003-BLG-262: FINITE-SOURCE EFFECTS FROM A POINT-MASS LENS \*

JAIYUL YOO<sup>1</sup>, D.L. DEPOY<sup>1</sup>, A. GAL-YAM<sup>2</sup>, B.S. GAUDI<sup>3</sup>, A. GOULD<sup>1</sup>, C. HAN<sup>4</sup>, Y. LIPKIN<sup>2</sup>, D. MAOZ<sup>2</sup>, E.O. OFEK<sup>2</sup>, B.-G. PARK<sup>5</sup>,  
AND R.W. POGGE<sup>1</sup>

(THE  $\mu$ FUN COLLABORATION)

AND

A. UDALSKI<sup>6</sup>, I. SOSZYŃSKI<sup>6</sup>, Ł. WYRZYKOWSKI<sup>6</sup>, M. KUBIAK<sup>6</sup>, M. SZYMAŃSKI<sup>6</sup>, G. PIETRZYŃSKI<sup>6</sup>, O. SZEWCZYK<sup>6</sup>, AND  
K. ŻEBRUŃ<sup>6</sup>

(THE OGLE COLLABORATION)

*accepted for publication in the Astrophysical Journal*

## ABSTRACT

We analyze OGLE-2003-BLG-262, a relatively short,  $t_E = 12.5 \pm 0.1$  day, microlensing event generated by a point-mass lens transiting the face of a K giant source in the Galactic bulge. We use the resulting finite-source effects to measure the angular Einstein radius,  $\theta_E = 195 \pm 17 \mu\text{as}$ , and so constrain the lens mass to the full-width half-maximum interval  $0.08 < M/M_\odot < 0.54$ . The lens-source relative proper motion is  $\mu_{\text{rel}} = 27 \pm 2 \text{ km s}^{-1} \text{ kpc}^{-1}$ . Both values are typical of what is expected for lenses detected toward the bulge. Despite the short duration of the event, we detect marginal evidence for a “parallax asymmetry”, but argue that this is more likely to be induced by acceleration of the source, a binary lens, or possibly by statistical fluctuations. Although OGLE-2003-BLG-262 is only the second published event to date in which the lens transits the source, such events will become more common with the new OGLE-III survey in place. We therefore give a detailed account of the analysis of this event to facilitate the study of future events of this type.

*Subject headings:* gravitational lensing — stars: low-mass

## 1. INTRODUCTION

Immediately following the announcement of the first microlensing detections (Alcock et al. 1993; Aubourg et al. 1993; Udalski et al. 1993), three groups independently showed that one could measure the microlens angular Einstein radius,

$$\theta_E = \sqrt{\kappa M \pi_{\text{rel}}}, \quad \kappa \equiv \frac{4G}{c^2 \text{AU}} \simeq 8 \frac{\text{mas}}{M_\odot}, \quad (1)$$

from the deviations on the microlensing lightcurve induced by the finite size of the source (Gould 1994a; Nemiroff & Wickramasinghe 1994; Witt & Mao 1994). Here  $M$  is the mass of the lens and  $\pi_{\text{rel}}$  is the lens-source relative parallax. Although all three considered the case of a point-mass lens passing close to or over the face of the source star, the great majority of the actual  $\theta_E$  measurements made over the ensuing decade used binary-lens events in which the source passed over the binary caustic (Albrow et al. 1999a, 2000a, 2001; Afonso et al. 2000; Alcock et al. 2000; An et al. 2002). There has been only one single-lens event for which finite-source effects have yielded a measurement of

$\theta_E$ . This was the spectacular event MACHO-95-30, whose M4 III source of radius  $r_* \sim 60 r_\odot$  was transited by the lens (Alcock et al. 1997). In fact, of the more than 1000 single-lens microlensing events discovered to date, only two have a measured  $\theta_E$  by any technique. The other was the equally spectacular MACHO-LMC-5 whose source-lens relative proper motion  $\mu_{\text{rel}}$  was measured by directly imaging and resolving the source and the M-dwarf lens six years after the event (Alcock et al. 2001). The angular Einstein radius was then inferred from,

$$\theta_E = \mu_{\text{rel}} t_E, \quad (2)$$

where  $t_E$  is the Einstein crossing time, which had been measured during the event.

Measurements of  $\theta_E$  are important because they constrain the physical properties of the lens. For most events, the only measured parameter that is related to the physical properties of the lens is  $t_E$ , which (from eqs. [1] and [2]) is a combination of three such properties,  $M$ ,  $\pi_{\text{rel}}$ , and  $\mu_{\text{rel}}$ . If  $\theta_E$  is measured, one then determines  $\mu_{\text{rel}}$  from equation (2), and the only remaining ambiguity is between  $M$  and  $\pi_{\text{rel}}$  (see eq. [1]). In some cases,  $\mu_{\text{rel}}$  is directly of interest. For example, measurement of the proper motion of the binary event MACHO-98-SMC-1 led to the conclusion that the lens was in the SMC itself rather than the Galactic halo (Afonso et al. 2000).

In other cases, one can combine the measurement of  $\theta_E$  with other measurements or limits to further constrain the character of the lens. The most dramatic example of this would be measurement of the microlens parallax,

$$\pi_E = \sqrt{\frac{\pi_{\text{rel}}}{\kappa M}}, \quad (3)$$

which can be determined either by observing the event from a satellite in solar orbit (Refsdal 1966; Gould 1995) or from the distortion of the microlens lightcurve induced by the accelerated motion of the Earth (Gould 1992). If both  $\theta_E$  and  $\pi_E$  are

<sup>1</sup> Department of Astronomy, The Ohio State University, 140 West 18th Avenue, Columbus, OH 43210; jaiyul, depoy, gould, pogge@astronomy.ohio-state.edu

<sup>2</sup> School of Physics and Astronomy and Wise Observatory, Tel Aviv University, Tel Aviv 69978, Israel; avishay, yiftah, dani, eran@wise.tau.ac.il

<sup>3</sup> Harvard-Smithsonian Center for Astrophysics, Cambridge, MA 02138; sgaudi@cfa.harvard.edu

<sup>4</sup> Department of Physics, Institute for Basic Science Research, Chungbuk National University, Chongju 361-763, Korea; cheongho@astroph.chungbuk.ac.kr

<sup>5</sup> Korea Astronomy Observatory, 61-1, Whaam-Dong, Youseong-Gu, Daejeon 305-348, Korea; bgpark@boao.re.kr

<sup>6</sup> Warsaw University Observatory, Al. Ujazdowskie 4, 00-478 Warszawa, Poland; udalski, soszynski, wyrzykow, mk, msz, pietrzym, szewczyk, zebrun@astrouw.edu.pl

\* Based in part on observations obtained with the 1.3 m Warsaw Telescope at the Las Campanas Observatory of the Carnegie Institution of Washington.

measured, one completely solves the event. That is,

$$M = \frac{\theta_E^2}{\kappa \pi_{\text{rel}}}, \quad \pi_{\text{rel}} = \theta_E \pi_E. \quad (4)$$

Unfortunately, while  $\pi_E$  has been measured for about a dozen events, only one of these also has a firm measurement of  $\theta_E$  (An et al. 2002), although Smith, Mao, Woźniak (2003) also obtained tentative measurements of both  $\theta_E$  and  $\pi_E$ .

Another type of constraint that can be combined with a measurement of  $\theta_E$  is an upper limit on the lens flux, which can often be obtained from the lightcurve. This flux limit can be converted into a luminosity limit at each possible lens distance. If the lens is assumed to be a main-sequence star, then using equation (1) and some reasonable assumption about the source distance, one can put an upper limit on the lens mass (e.g., Albrow et al. 2000b). Even in the absence of any additional constraints, equation (1) can be combined with a Galactic model to make statistical statements about the lens properties (e.g., Alcock et al. 1997).

The principal reason that most  $\theta_E$  measurements come from binary lenses and that single-lens measurements are extremely rare is that the ratio  $\rho$ , of the angular source radius,  $\theta_*$ , to the Einstein radius,

$$\rho \equiv \frac{\theta_*}{\theta_E}, \quad (5)$$

is usually extremely small. At the distance of the Galactic bulge, even a clump giant has an angular radius  $\theta_* \sim 6 \mu\text{as}$ , and main-sequence stars are an order of magnitude smaller. By contrast, typical Einstein radii are  $\theta_E \sim 310 \mu\text{as} [(M/0.3M_\odot)(\pi_{\text{rel}}/40 \mu\text{as})]^{1/2}$ . Hence, the probability that the lens will pass directly over the source, which is what is required for substantial finite source effects (Gould & Welch 1996), is very small. By contrast, binary lenses, with their extended caustic structures, have a much higher probability of generating finite-source effects.

However, new microlensing surveys are beginning to alter this situation. In particular, the new phase of the Optical Gravitational Lens Experiment, OGLE-III (Udalski et al. 2002a), with its dedicated 1.3 m telescope and new  $35' \times 35'$  field,  $0''.26$  pixel, mosaic CCD camera and generally excellent image quality is generating microlensing alerts at the rate of 500/season (as reported by the OGLE-III Early Warning System, EWS, <http://www.astrouw.edu.pl/~ogle/ogle3/ews/ews.html>), roughly an order of magnitude higher than previous surveys. This high event rate is itself enough to overcome the low,  $\mathcal{O}(\rho)$ , probability of a source-crossing event, and so to generate a few finite-source affected EWS alerts per year. Moreover, because EWS relies on image-subtraction (Woźniak 2000), it is sensitive to extremely high magnification events of relatively faint sources, which have a higher chance of a source crossing than do typical events.

OGLE-III is able to generate this high event rate only by reducing its visits to individual fields below 1/night. Hence, it would not customarily observe the alerted event during the lens transit of the source. However, several groups, including the Probing Lensing Anomalies NETwork (PLANET, Albrow et al. 1998), the Microlensing Planet Search (MPS, Rhie et al. 1999), and the Microlensing Follow-Up Network ( $\mu\text{FUN}$ , <http://www.astronomy.ohio-state.edu/~microfun/>) intensively monitor alerts from EWS and also from the Microlensing Observations in Astrophysics collaboration (MOA, Bond et al. 2001), primarily to search for planets.

High-magnification events are the most sensitive to planetary perturbations (Gould & Loeb 1992; Griest & Safizadeh 1998), so these groups tend to focus on these events, particularly their peaks. As a consequence, there is a good chance they will detect finite-source effects when they occur. Moreover, OGLE-III diverts time from its regular field rotation (survey mode) to especially interesting events (follow-up mode) and so can itself also directly detect these effects.

Here we report observations of EWS alert OGLE-2003-BLG-262, which exhibited clear indications of finite-source effects near its peak on 2003 July 19. By fitting this event to a single-lens finite-source model, we measure the  $\theta_E$  and so  $\mu_{\text{rel}}$ . We use this information, combined with a measurement of  $t_E$  to constrain the mass of the lens. We also present marginal ( $\gtrsim 3\sigma$ ) evidence for an asymmetry which, if due to parallax effects, would imply that the lens was a brown dwarf. However, we argue that the observed asymmetry is either due to statistical fluctuations, a weak binary lens, or acceleration of the source. Our analysis provides a framework in which to analyze future finite-source single-lens event, which should be considerably more common due to the higher rate of alerted events.

## 2. OBSERVATIONAL DATA

The microlensing event OGLE-2003-BLG-262 was identified by the OGLE-III EWS (Udalski et al. 1994) on 2003 June 26, i.e., more than three weeks before peak, which occurred on  $\text{HJD}' \equiv \text{HJD} - 2450000 = 2839.84$  over the Pacific Ocean. OGLE-III observations were carried out with the 1.3-m Warsaw telescope at the Las Campanas Observatory, Chile, which is operated by the Carnegie Institution of Washington. These comprise a total of 170 observations in  $I$  band, including 68 in the 2001 and 2002 seasons. The exposures were generally the standard 120 s, except for three special 40 s exposures on the peak and following night when the star was too bright for the standard exposure time. Photometry was obtained with the OGLE-III image subtraction technique data pipeline (Udalski et al. 2002a) based in part on the Woźniak (2000) DIA implementation. The source had also been monitored by OGLE-II and was found to be very stable over four previous seasons (April 1997 – October 2000).

Following the alert, the event was monitored by  $\mu\text{FUN}$  from sites in Chile and Israel. The Chile observations were carried out at the 1.3m (ex-2MASS) telescope at Cerro Tololo InterAmerican Observatory, using the ANDICAM, which simultaneously images at optical and infrared wavelengths (DePoy et al. 2003). During the seven nights from  $\text{HJD}' 2838.5$  to  $2844.8$ , there were a total of 45 observations in  $I$ , 4 in  $V$ , and 28 in  $H$ . The  $I$  and  $V$  observations were generally 300 s, although the exposures were shortened to 120 s during the three nights from  $2839.6$  to  $2841.8$ . The individual  $H$  observations were 60 s and were grouped in 5 dithered exposures, which were taken simultaneously with one 300 s  $V$  or  $I$  exposure or with two 120 s  $I$  exposures. All images were flat fielded using sky flats for  $V$  and  $I$ , and dome flats for  $H$ . Photometry was obtained with DoPHOT (Schechter, Mateo & Saha 1993) for all  $V$ ,  $I$ , and  $H$  images.

After reductions, the contiguous groups of 5 (or 10 in the case of back-to-back  $V$  and  $I$  exposures)  $H$  points were averaged into single data points to yield the above-stated 28 points.

The  $\mu\text{FUN}$  Israel observations were carried out on the Wise 1m telescope at Mitzpe Ramon, 200 km south of Tel-Aviv, roughly  $105^\circ$  east of Chile. During the nights of  $\sim 2839.3$ ,  $\sim$

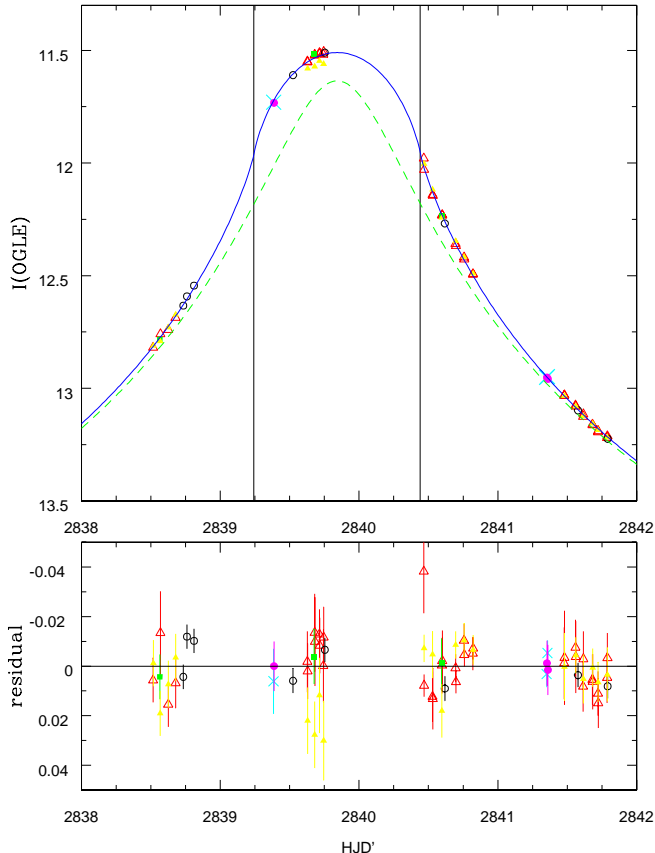


FIG. 1.— Photometry of microlensing event OGLE-2003-BLG-262 near its peak on 2003 July 19.34 (HJD 2452839.83). Data points are in  $I$  (OGLE: empty circles;  $\mu$ FUN Chile: empty triangles;  $\mu$ FUN Israel: crosses),  $V$  ( $\mu$ FUN Chile: filled squares;  $\mu$ FUN Israel: filled circles), and  $H$  ( $\mu$ FUN Chile: filled triangles). All bands are linearly rescaled so that  $F_s$  and  $F_b$  are the same as the OGLE observations, which define the magnitude scale. When the lens is close to or inside (vertical lines) the source, the lightcurves are expected to differ due to limb darkening (LD). The solid curve shows the best fit model for the  $I$ -band curve. The fact that the  $H$ -band points near the peak are below this curve is in qualitative accord with the lower LD in  $H$  compared to  $I$ . The dashed curve shows the lightcurve expected for the same lens model, but a point source.

2841.3, and  $\sim 2842.3$ , there were a total of four observations in  $I$  and three in  $V$ . The exposures (all 240 s) were obtained using the Wise Tektronix 1K CCD camera. Data were flat-fielded and zero corrected in the usual way, and photometry obtained with DoPHOT.

The position of the source is R.A. =  $17^{\text{h}}57^{\text{m}}08^{\text{s}}51$ , decl. =  $-30^{\circ}20'05''.1$  (J2000) ( $l, b = 0.41918, -3.46935$ ), and so was accessible for most of the nights near peak from Chile, but only a few hours from Israel. Unfortunately, due to a communications mixup,  $\mu$ FUN Chile observations on the peak night were bunched in a narrow time interval. Happily, when these are combined with the two OGLE observations and the one  $I$ -band and one  $V$ -band  $\mu$ FUN Israel observations, the rising half of the peak is still clearly traced out. See Figure 1.

We emphasize that while three of the datasets have relatively few points, two of these small datasets actually play crucial roles. The three post-peak  $\mu$ FUN Israel  $I$  points serve to align this dataset with the two larger  $I$  datasets and so enable the first point (on 2839.38) to directly test the near-peak finite-source profile, which otherwise would be determined by

a single compact set of points. See Figure 1. The four  $\mu$ FUN Chile  $V$  points allow determination of the color of the source and so permit one to estimate the source size and thus the proper motion and angular Einstein radius. See § 4. With only three points, two of which are nearly coincident, the  $\mu$ FUN Israel  $V$  data do not contribute significantly to the fit because they are absorbed by two fitting parameters,  $F_s$  and  $F_b$ . However, they are included here for completeness.

The source lies in one of the OGLE-II calibrated photometry fields (Udalski et al. 2002b) (<ftp://bulge.princeton.edu/ogle/ogle2/maps/bulge/>) and this allows us to place it on a calibrated color magnitude diagram. See Figure 2. The source lies on the red giant branch, about 1 mag brighter than the clump and about 0.2 mag redder. It therefore has considerably larger angular radius than typical microlens sources, and this, together with the high magnification of the event, considerably increased the chance for significant finite source effects.

Sumi et al. (2003) measured the proper motion of the source (relative to the frame of the Galactic bulge) and found  $(\mu_{\alpha,s}, \mu_{\delta,s}) = (0.45 \pm 0.41, -5.75 \pm 0.40)$  mas yr $^{-1}$ . When corrected to the Tycho-2 frame, this becomes  $(\mu_{\alpha,s}, \mu_{\delta,s}) = (-2.9, -12.4)$  mas yr $^{-1}$ .

### 3. FORMALISM

#### 3.1. Finite-Source Effects

In most cases, the lensed star is regarded as a point source because the angular size of the source is negligibly small compared to the angular separation of the source and the lens. The magnification is then given by (Paczynski 1986),

$$A(u) = \frac{u^2 + 2}{u(u^2 + 4)^{1/2}}, \quad (6)$$

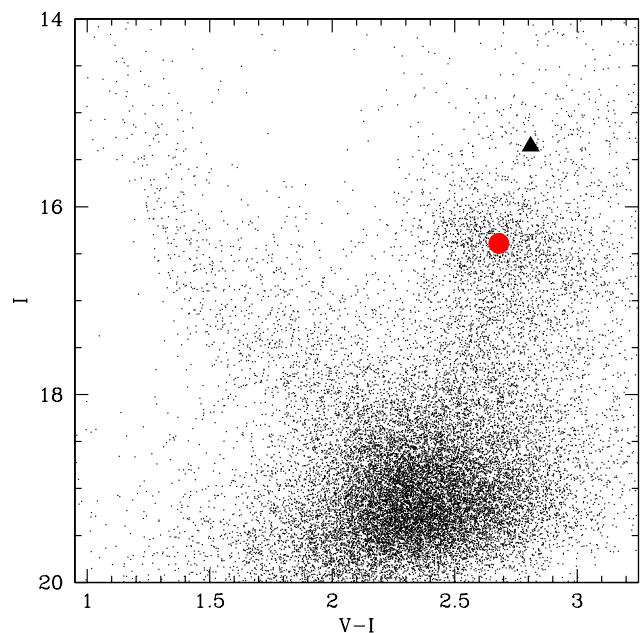


FIG. 2.— Calibrated color-magnitude diagram (CMD) of a  $10'$  square around OGLE-2003-BLG-262 taken from OGLE-II photometry well before the event. The source (marked with a black triangle) is about 1 mag brighter and 0.2 mag redder than the centroid of the clump giants (marked with a red circle). The fit shows negligible blending, so the apparent source position on the CMD is virtually identical to its true (deblended) position.

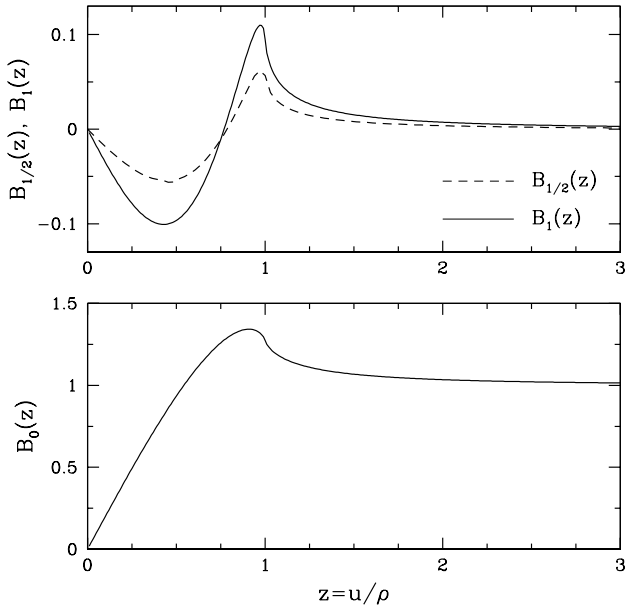


FIG. 3.— Finite source functions  $B_0(z)$ ,  $B_{1/2}(z)$  and  $B_1(z)$  given by eqs. (10), (19) and (16). For  $\rho \ll 1$ , the limb-darkened magnification is very well represented by  $A_{\text{ld}}(u|\rho) = A(u)[B_0(z) - \Gamma B_1(z)]$ , where  $\rho$  is the source size and  $u$  is the lens-source separation, both in units of  $\theta_E$ ,  $\Gamma$  is the linear limb-darkening coefficient, and  $z = u/\rho$ .

where  $u$  is the projected source-lens separation in units of the angular Einstein radius  $\theta_E$ . However, this approximation breaks down for  $u \lesssim \rho$ . Finite-source effects then dominate.

If the source were of uniform brightness, the total magnification would simply be the mean magnification over the source,

$$A_{\text{uni}}(u|\rho) = W_0 \left[ (u/\rho) | \rho; A(x) \right], \quad (7)$$

where

$$W_n \left[ z | \rho; f(x) \right] \equiv \frac{1}{\pi} \int_0^{2\pi} d\theta \int_0^1 dr r (1-r^2)^{n/2} f(\rho \sqrt{r^2 + z^2 - 2rz \cos \theta}). \quad (8)$$

Witt & Mao (1994) gave an exact evaluation of this expression in closed, albeit cumbersome, form. Gould (1994a) advocated a simple approximation to equation (8),

$$A_{\text{uni}}(u|\rho) \simeq A(u) B_0(u/\rho), \quad B_0(z) \equiv z \rho W_0 \left[ z | \rho; x^{-1} \right], \quad (9)$$

which follows from the fact that  $A(u) \simeq u^{-1}$  when  $u \ll 1$ . Note that  $B_0$  depends on  $\rho$  only through the ratio  $z = u/\rho$ . However, Gould (1994a) did not explicitly evaluate  $B_0$  nor did he demonstrate the range of validity of the approximation (9). It is straightforward to show that,

$$B_0(z) = \frac{4}{\pi} z E(k, z), \quad k \equiv \min(z^{-1}, 1), \quad (10)$$

where  $E$  is the incomplete elliptic integral of the second kind, and where we follow the notation of Gradshteyn & Ryzhik (1965). Using the expansion  $A(u) = u^{-1} [1 + (3/8)u^2 + \dots]$ , and after some algebra, one may show that to second order in  $\rho$ ,

$$A_{\text{uni}}(u|\rho) = A(u) B_0(z) \left[ 1 + \frac{\rho^2}{8} Q(z) \right], \quad z \equiv \frac{u}{\rho}, \quad (11)$$

where,

$$Q(z) = \frac{1}{3} \left[ 7 - 8z^2 - 4(1-z^2) \frac{F(k, z)}{E(k, z)} \right], \quad (12)$$

and where  $F$  is the incomplete elliptic integral of the first kind. We find numerically that  $-0.38 \leq Q(z) \leq 1$ , where the limits are saturated at  $z = 0.97$  and  $z = 0$  respectively. For OGLE-2003-BLG-262,  $\rho^2/8 \lesssim 5 \times 10^{-4}$ , which is about an order of magnitude smaller than our photometric errors. The zeroth-order approximation (9) is therefore appropriate here and, we believe, is likely to be appropriate in most other cases as well.

### 3.2. Limb Darkening

Real stars are not uniform, but rather are limb-darkened. For simplicity and also because the quality of the data does not warrant a more sophisticated treatment, we adopt a one-parameter linear limb-darkening law for the surface brightness of the source,

$$S_\lambda(\vartheta) = \bar{S}_\lambda \left[ 1 - \Gamma_\lambda \left( 1 - \frac{3}{2} \cos \vartheta \right) \right], \quad (13)$$

where  $\vartheta$  is the angle between the normal to the stellar surface and the line of sight,  $\bar{S}_\lambda$  is the mean surface brightness of the source, and the  $\Gamma_\lambda$  is the limb-darkening (LD) coefficient for a given wavelength band  $\lambda$ . The factor  $3/2$  originates from our requirement that the total flux be  $F_{\text{tot}, \lambda} = \pi \theta_*^2 \bar{S}_\lambda$ .

The LD magnification is then (exactly),

$$A_{\text{ld}}(u|\rho) = W_0 \left[ (u/\rho) | \rho; A(x) \right] - \Gamma \left\{ W_0 \left[ (u/\rho) | \rho; A(x) \right] - 1.5 W_1 \left[ (u/\rho) | \rho; A(x) \right] \right\}. \quad (14)$$

However, we adopt the same simplifying approximation as above and write,

$$A_{\text{ld}}(u|\rho) \simeq A(u) [B_0(z) - \Gamma B_1(z)], \quad (15)$$

where

$$B_1(z) = B_0(z) - \frac{3}{2} z \rho W_1 \left[ z | \rho; x^{-1} \right]. \quad (16)$$

Figure 3.1 shows  $B_0$ ,  $B_{1/2}$  (see below) and  $B_1$  as functions of  $z$ . Note that  $B_0(z) \rightarrow 1$  and  $B_1(z) \rightarrow 0$  in the limit  $z \rightarrow \infty$  so that the magnification (eq. [15]) reduces to the point-source case. In the opposite limit,  $z \rightarrow 0$ , equations (10) and (16) reduce to  $B_0(z) \rightarrow 2z$  and  $B_1(z) \rightarrow (2 - 3\pi/4)z$ , so that  $A_{\text{fin}}(0) = 2/\rho [1 + (3\pi/8 - 1)\Gamma]$ . Hence, the peak magnification depends primarily on  $\rho$  and only weakly on  $\Gamma$ .

In high-precision LD measurements, it is generally accepted that a two-parameter square-root LD law is more appropriate to describe brightness profiles of stars (Albrow et al. 1999a; Fields et al. 2003) than equation (13) although it is not used in the present work. Therefore, for completeness we extend the above formalism to a two-parameter square-root LD law in the form of

$$S_\lambda(\vartheta) = \bar{S}_\lambda \left[ 1 - \Gamma_\lambda \left( 1 - \frac{3}{2} \cos \vartheta \right) - \Lambda_\lambda \left( 1 - \frac{5}{4} \cos^{1/2} \vartheta \right) \right], \quad (17)$$

where  $\Lambda_\lambda$  is the additional LD coefficient for a given wavelength band  $\lambda$ . The magnification can then be approximated by,

$$A_{\text{sqtrld}}(u|\rho) \simeq A(u) [B_0(z) - \Gamma B_1(z) - \Lambda B_{1/2}(z)], \quad (18)$$

where

$$B_{1/2}(z) = B_0(z) - \frac{5}{4} z \rho W_{1/2} \left[ z | \rho; x^{-1} \right]. \quad (19)$$

TABLE 1. OGLE-2003-BLG-262 FIT PARAMETERS

Parameter	Free Fit		Fixed LD		Fixed LD & $\pi_E$	
	Value	Error	Value	Error	Value	Error
$t_0(\text{days})$ .....	2839.8411	0.0015	2839.8415	0.0015	2839.8424	0.0014
$u_0$ .....	0.0365	0.0005	0.0362	0.0004	0.0360	0.0004
$t_E(\text{days})$ .....	12.5309	0.0945	12.5568	0.0941	12.6181	0.0916
$\rho$ .....	0.0605	0.0010	0.0599	0.0005	0.0595	0.0005
$\Gamma_V$ .....	0.8515	0.2069	0.7200	-	0.7200	-
$\Gamma_I$ .....	0.6118	0.1499	0.4400	-	0.4400	-
$\Gamma_H$ .....	0.0975	0.2028	0.2600	-	0.2600	-
$\pi_{E,\parallel}$ .....	-0.8572	0.3130	-0.8335	0.3120	0.0000	-
$(F_b/F_s)_{I_1}$ .....	-0.0011	0.0095	0.0028	0.0093	0.0083	0.0091
$(F_b/F_s)_{I_2}$ .....	-0.0275	0.0175	-0.0134	0.0172	-0.0027	0.0168
$(F_b/F_s)_{I_3}$ .....	0.1865	0.0783	0.2283	0.0746	0.2361	0.0749
$(F_b/F_s)_{V_2}$ .....	0.0122	0.0481	0.0192	0.0478	0.0296	0.0479
$(F_b/F_s)_{V_3}$ .....	0.0406	0.1688	0.1251	0.1465	0.1191	0.1473
$(F_b/F_s)_H$ .....	-0.0048	0.0176	-0.0114	0.0175	-0.0009	0.0172
$\chi^2$ .....	233.50	-	252.66	-	259.76	-

NOTE. — Observatories: 1=OGLE, 2= $\mu$ FUN Chile, 3= $\mu$ FUN Israel

### 3.3. Parallax Effects

Microensing events are fit to

$$F(t) = F_s A[u(t)] + F_b, \quad (20)$$

where  $F_s$  is the source flux,  $F_b$  is the blended background light, and

$$u(t) = \sqrt{[\tau(t)]^2 + [\beta(t)]^2}. \quad (21)$$

Conventionally, rectilinear motion is assumed,

$$\tau(t) = \frac{t - t_0}{t_E}, \quad \beta(t) = u_0. \quad (22)$$

Hence, the simplest fit has five parameters,  $F_s$ ,  $F_b$ , the impact parameter  $u_0$ , the time of closest approach  $t_0$ , and the Einstein timescale  $t_E$ . However, even if the source and lens are in rectilinear motion, the Earth is not. Thus, strictly speaking one should write

$$\tau(t) = \frac{t - t_0}{t_E} + \pi_{E,\parallel} a_{\parallel}(t) + \pi_{E,\perp} a_{\perp}(t), \quad (23)$$

$$\beta(t) = u_0 - \pi_{E,\parallel} a_{\perp}(t) + \pi_{E,\perp} a_{\parallel}(t). \quad (24)$$

Here  $a \equiv (a_{\parallel}, a_{\perp})$  is the difference in the Earth's position (projected onto the plane of the sky and measured in AU) relative to what it would have been had the Earth maintained the velocity it had had at  $t_0$ , and the  $a_{\parallel}$  direction is defined by the direction of the Earth's (projected) acceleration at  $t_0$ .

Choosing the Earth frame at the peak of the event as the inertial frame is certainly not standard procedure. It is more common, and mathematically more convenient, to use the Sun's frame. However, for relatively short events  $t_E \lesssim \text{yr}/2\pi$ , the parallax effect is quite weak, and it is only possible to measure one component of  $\pi_E = (\pi_{E,\parallel}, \pi_{E,\perp})$ , namely the parallax asymmetry, which is the component  $(\pi_{E,\parallel})$  of the parallax parallel to the Earth's projected acceleration at the peak of the event (Gould, Miralda-Escudé & Bahcall 1994). In this case,  $u_0$ ,  $t_0$ , and  $t_E$  as seen from the Earth at the event peak are very well defined by the fit to the event without parallax, whereas these quantities as seen from the Sun are impossible to determine. For these short events,  $a_{\perp} \sim 0$ , and the impact of  $a_{\parallel}$  through  $\beta$  is undetectable because it is absorbed into  $u_0$ ,  $t_E$ ,  $F_s$ , and  $F_b$ . Equations (23) and (24) then reduce to,

$$\tau(t) = \frac{t - t_0}{t_E} + \pi_{E,\parallel} a_{\parallel}(t), \quad \beta(t) = u_0. \quad (25)$$

### 4. MODEL FITTING

We begin by fitting the event taking account of both LD and parallax. There are then a total of 20 free parameters: 12 parameters for  $F_s$  and  $F_b$  from each of the six observatory/filter combinations, 3 LD parameters, one each for  $I$ ,  $V$  and  $H$ , the basic microlensing parameters  $t_0$ ,  $u_0$ , and  $t_E$ , as well as the source size,  $\rho$ , and the parallel component of the parallax,  $\pi_{E,\parallel}$ . We consider the possibility of a correction for seeing, but find no correlation of the residuals of the  $\mu$ FUN Chile  $I$  or  $H$  data with seeing. The source is quite bright (see Fig. 2) and it is virtually unblended (see below), so it is quite plausible that there would be no seeing correlations. We set a minimum error of 0.003 magnitudes for all observations, regardless of what value the photometry programs report. We then rescale the errors for the OGLE,  $\mu$ FUN Chile  $I$ , and  $H$  by factors of 1.62, 1.12, and 1.83 respectively, in order to force  $\chi^2/\text{dof}$  to unity. There are too few points in each of the remaining observatory/filter combinations to permit accurate rescalings, and the actual total  $\chi^2$  values for these are consistent with the reported errors being correct.

We minimize  $\chi^2$  using Newton's method (e.g., Press et al. 1992), which guarantees that one has found a local minimum because the derivative of  $\chi^2$  with respect to each parameter is zero. In contrast to caustic-crossing binary lenses (Albrow et al. 1999b; Dominik 1998), and to space-based (Gould 1994b; Refsdal 1966) and ground-based (Smith, Mao & Paczyński 2003) parallax measurements for which there can be multiple local minima, standard microlensing (even when modified by inclusion of finite-source effects) is expected to have a single global minimum. We nevertheless checked for multiple minima by adopting several initial trial solutions that were consistent with point-source/point-lens fits to a data set that excluded the peak. All converged to the same solution.

We initially allow the three LD coefficients to be free parameters. We find fit values and errors  $(\Gamma_V, \Gamma_I, \Gamma_H) = (0.85 \pm 0.21, 0.61 \pm 0.15, 0.10 \pm 0.20)$  (see Tab. 1). These errors are all relatively large. The values therefore appear only mildly inconsistent with those of EROS-BLG-2000-5,  $(\Gamma_V, \Gamma_I, \Gamma_H) = (0.72, 0.44, 0.26)$  (Fields et al. 2003), a slightly redder source with much better measured LD. It is then somewhat shocking

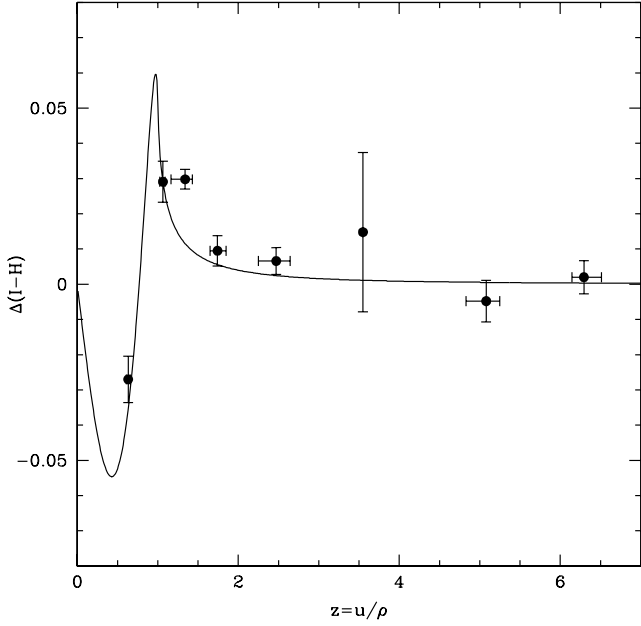


FIG. 4.— Model-independent color changes due to limb-darkening. A linear regression of  $H$  on  $I$  flux is performed at high  $z$  ( $z > 1.7$ ) to put the two passbands on the same scale and to remove the small blending difference. Then  $I-H$  is measured at each point and the measurements for each day are averaged, except for  $\text{HJD}' \sim 2840.5$ , ( $z \sim 1.25$ ), which is broken into two bins. The curve is  $0.5B_1(z)$ , which is the expected form of this magnitude difference for a linear limb-darkening difference  $\Gamma_I - \Gamma_H = 0.5$ .

to discover that there is a net penalty of  $\Delta\chi^2 = 19$  for enforcing the EROS-BLG-2000-5 LD values. A major part of the problem is that while the errors in the individual LD parameters are large, the data strongly demand a large LD difference  $\Delta\Gamma = \Gamma_I - \Gamma_H = 0.51 \pm 0.09$  when  $\Gamma_I$  is held fixed at 0.44. That is, although the errors on the individual determinations of  $\Gamma_I$  and  $\Gamma_H$  are large, they are strongly correlated, such that the difference  $\Delta\Gamma$  is much better determined. This in turn can be traced to the fact that there is a color offset  $\Delta(I-H) = -0.03$  at the peak, which is clearly visible in Figure 1 and which the fitting routine ascribes to the source having much more LD in  $I$  than  $H$  and hence being relatively blue in the center. See Figure 4. However, since the measurement seems to contradict what is otherwise known about LD, and derives primarily from a single cluster of data points, which may be subject to common systematic error, we choose to fix the three  $\Gamma$ 's at the above stated EROS-BLG-2000-5 values. We thereby lose any independent LD information. This is not a major loss since our errors are too large to be competitive with other measurements (e.g. Fields et al. 2003). Our main concern is that whatever problem may be corrupting the LD could also impact the measurement of the parameters that we are most interested in measuring, which are principally  $\rho$  and  $t_E$ . In fact, by enforcing these  $\Gamma$ 's,  $\rho$  is changed by only 1.6% and  $t_E$  by only 0.3%. Since enforcing the LD parameters has no practical consequences (other than the loss of LD information), we adopt the EROS-BLG-2000-5 value.

We then find,

$$\rho = 0.0599 \pm 0.0005, \quad t_E = 12.557 \pm 0.094 \text{ days.} \quad (26)$$

Figure 1 shows the fit to the data in the region of the peak. All six observatory/band combinations have been linearly

rescaled to have an  $F_s$  and  $F_b$  equal to those of the OGLE data set. The three  $I$  band data streams should then follow the same lightcurve, whose best fit model is shown by the solid curve. However, the  $V$  and  $H$  band points should deviate from this curve during the source crossing,  $|t - t_0| \lesssim \rho t_E = 0.76$  days, because of LD. There are not enough data in the  $V$  band to test this. As mentioned above, the  $H$  band cluster of points near the peak clearly lies below the curve, probably by too much.

We measure a parallax asymmetry,

$$\pi_{E,\parallel} = 0.83 \pm 0.31. \quad (27)$$

That is, parallax is formally detected at the  $3\sigma$  level. More specifically,  $\Delta\chi^2 = 7$  relative to enforcing  $\pi_{E,\parallel} = 0$ . To illustrate the strength (or lack thereof) of this detection we show in Figure 5 the fit to the data enforcing  $\pi_{E,\parallel} = 0$ . The lower panel of this figure shows the residuals together with their expected form for  $\pi_{E,\parallel} = 1$ . When we first constructed this figure on about  $\text{HJD}' = 2870$ , we realized that there might still be time to test the reality of this parallax detection. OGLE observations were then intensified from one every several days to one or two per day. These additional observations did not tend to confirm the detection, but also did not firmly contradict it. Hence, the parallax detection remains ambiguous. All previous events with firm parallax detections had Einstein timescales at least 5 times longer than this one, so it would have been remarkable if we had obtained a robust detection.

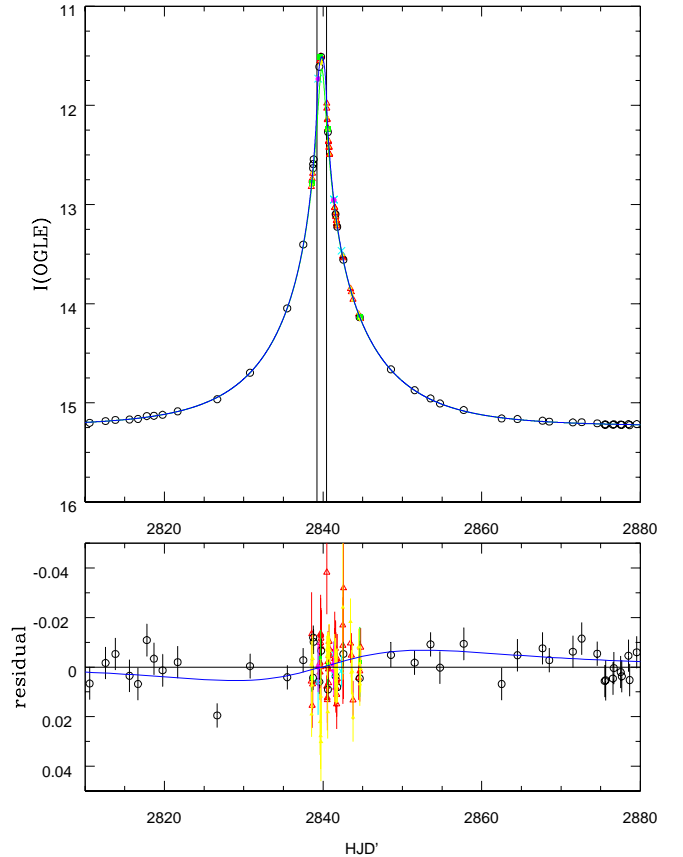


FIG. 5.— Similar to Fig. 1, but now a full view of the lightcurve of OGLE-2003-BLG-262 over about 5 Einstein timescales. The fit does not include parallax, and the residuals (lower panel) show an asymmetry such as would be induced by acceleration of the Earth parallel to the direction of lens motion (solid curve).

Moreover, as we discuss in § 6, the sign of the effect is opposite to what would be produced by the expected lens-source kinematics, while the effect itself could be produced by xallarap or by lens binarity.

The errors shown in Table 1 are  $\sqrt{c_{ii}}$  where  $c_{ij}$  is the  $ij$ -th element of covariant matrix, and the correlation coefficients defined as  $\tilde{c}_{ij} \equiv c_{ij}/\sqrt{c_{ii}c_{jj}}$  are,

$$\begin{pmatrix} 1.0000 & 0.2000 & -0.0675 & -0.1441 & 0.2288 & 0.1139 \\ 0.2000 & 1.0000 & -0.8463 & 0.7969 & -0.1861 & 0.8972 \\ -0.0675 & -0.8463 & 1.0000 & -0.9244 & 0.2790 & -0.9793 \\ -0.1441 & 0.7969 & -0.9244 & 1.0000 & -0.2990 & 0.9086 \\ 0.2288 & -0.1861 & 0.2790 & -0.2990 & 1.0000 & -0.2467 \\ 0.1139 & 0.8972 & -0.9793 & 0.9086 & -0.2467 & 1.0000 \\ -0.1137 & -0.8971 & 0.9758 & -0.9060 & 0.2531 & -0.9986 \end{pmatrix}, \quad (28)$$

where parameters are  $t_0$ ,  $u_0$ ,  $t_E$ ,  $\rho$ ,  $\pi_{E,\parallel}$ ,  $(F_s)_{I_1}$ , and  $(F_b)_{I_1}$ . As expected from experience with standard microlensing events,  $F_s$  and  $F_b$  are extremely correlated, and these are both highly correlated with  $u_0$  and  $t_E$ . What is new in equation (28) is that  $\rho$  is also highly correlated with these other four parameters. The fundamental reason for this is that all five of these parameters are symmetric in  $(t - t_0)$ . By contrast  $\pi_{E,\parallel}$  is only weakly correlated with the other parameters.

## 5. CONSTRAINTS ON THE EVENT

### 5.1. Angular Einstein Radius $\theta_E$

As discussed by Albrow et al. (2000a), one can determine  $\theta_*$  from the source's dereddened color and magnitude  $[(V - I)_0, I_0]_s$  by first transforming from  $(V - I)_0$  to  $(V - K)_0$  using the color-color relations of Bessell & Brett (1988), and then applying the empirical relation between color and surface brightness to obtain  $\theta_*$  (van Belle 1999).

Again following Albrow et al. (2000a), we determine  $[(V - I)_0, I_0]_s$  from the measured offset of the unamplified source (as determined from the microlensing fit) relative to the centroid of the clump giants on an instrumental CMD, the latter's dereddened color and magnitude being regarded as “known”. We measure this offset to be

$$\Delta I = I_s - I_{\text{clump}} = -1.06, \quad \Delta(V - I) = (V - I)_s - (V - I)_{\text{clump}} = 0.15. \quad (29)$$

In general, the source may be blended, so that the  $V$  and  $I$  of the source derived from the microlensing fit will not necessarily agree with those of the object identified as the “source” in an image taken at baseline. Hence, one cannot in general derive the offset from a CMD constructed from such a baseline image. However, in this case, there is essentially no blending, so the offset in the baseline calibrated CMD shown in Figure 2 is virtually identical (within 0.02 mag) to that given in equation (29).

The “known” values of  $[(V - I)_0, I_0]_{\text{clump}}$  have recently come under dispute. The basic problem is that the previous calibrations of these quantities relied on a number of steps, in each of which it was assumed that the ratio of total to selective extinction was  $R_{VI} \equiv A_V/E(V - I) \sim 2.5$ . However, using this same value, Paczyński (1996) and Stutz, Popowski & Gould (1999) found respectively that the colors of bulge clump giants and RR Lyrae stars were anomalous relative to local populations. Popowski (2000) then proposed that these anomalies could be resolved if the dust toward this line of sight were itself anomalous, with  $R_{VI} \sim 2.1$ . Udalski (2003) then demonstrated that this was very likely the case based on OGLE-II data. While it would be both worthwhile and feasible to retrace all the steps

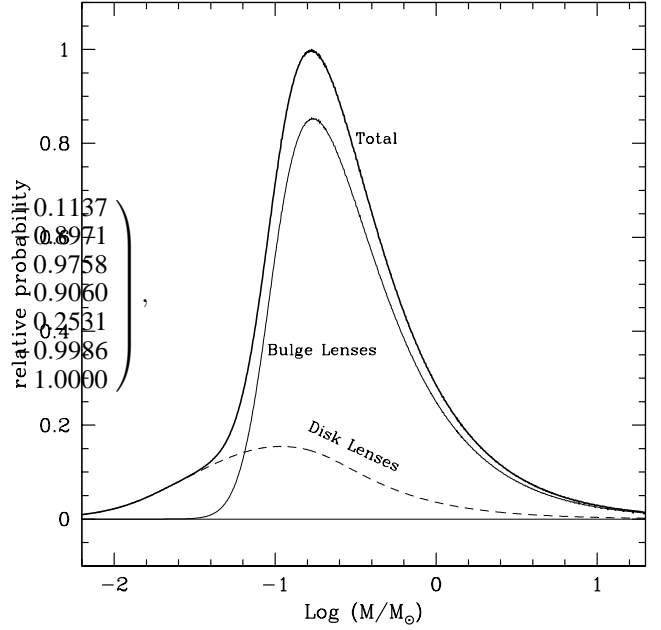


FIG. 6.— Constraints on the lens mass of OGLE-2003-BLG-262. The curves show the relative probability of different lens masses given the measurement of  $\theta_E = 195 \mu\text{as}$  and the mass distribution along the line of sight as predicted by the Han & Gould (1995, 2003) model. The solid and dashed curves show the probability for bulge-bulge and disk-bulge combinations of lenses and sources. The bold curve is their sum. The constraints arising from the determination of  $\mu_{\text{rel}}$  (equivalently  $t_E$ ) would be extremely weak and are not incorporated here.

that led to the old calibration in light of this revised  $R_{VI}$ , the magnitude of this project lies well beyond the scope of the present work. Pending such a revision, we adopt a simpler approach.

The distance to the Galactic center has now been measured geometrically by Eisenhauer et al. (2003) to be  $R_0 = 8.0 \pm 0.4$  kpc based on the “visual-binary” method of Salim & Gould (1999). Bulge stars are of similar metallicity to local stars, so the clump should be of similar color to the *Hipparcos* clump stars  $(V - I)_0 \sim 1.00$ . (Recall that it was the apparent failure of this expectation that led to the discovery of anomalous extinction.) The  $I$ -band luminosity of clump stars does not depend strongly on age (until the stars are so young that the turnoff luminosity approaches that of the horizontal branch). Hence, the bulge clump stars should have approximately the same  $M_I$  as the *Hipparcos* sample. For this we adopt  $M_I = -0.20$ , the value found by Paczyński & Stanek (1996) for their 70 pc sample (and prior to their reddening correction which we consider to be substantially too large.) Hence, in lieu of a more thoroughgoing calibration, we adopt

$$[(V - I)_0, I_0]_{\text{clump}} = (1.00, 14.32). \quad (30)$$

Combining equations (29) and (30) and applying the van Belle (1999) relation, we find

$$\theta_* = 11.7 \pm 1.0 \mu\text{as}, \quad (31)$$

where the error comes primarily from the 8.7% intrinsic scatter in the van Belle (1999) relation.

This evaluation would appear to depend on the assumption that the source suffers exactly as much extinction as a typical clump star, which it might not, either due to highly variable



extinction or to the source lying well in the foreground and so in front of a large fraction of the dust. In fact, if it were determined that the extinction toward the source were greater than to the clump by  $\Delta E(V-I) = 0.2$  or less by  $\Delta E(V-I) = -0.6$ , the estimate of  $\theta_*$  would change less than 3%. This is because the changes in the inferred surface brightness and luminosity lead to changes in the source-size estimate that go in opposite directions.

Combining equations (26) and (31), we obtain,

$$\theta_E = 195 \pm 17 \mu\text{as}, \quad (32)$$

$$\mu_{\text{rel}} = 5.63 \pm 0.49 \text{ mas yr}^{-1} = 26.7 \pm 2.3 \text{ km s}^{-1} \text{ kpc}^{-1}.$$

We now use this measurement of  $\theta_E$ , in conjunction with its definition, equation (1), to write the source-lens relative parallax as a function of the lens mass,

$$\pi_{\text{rel}}(M) = \frac{\theta_E^2}{\kappa M} = 4.8 \mu\text{as} \left( \frac{M}{M_\odot} \right)^{-1}. \quad (33)$$

Given a Galactic mass model along the line of sight,  $\rho(x)$ , the prior probability of a given relative parallax is proportional to

$$P(\pi_{\text{rel}}) \propto \int_0^\infty dD_s D_s^2 \rho(D_s) \int_0^{D_s} dD_l D_l \rho(D_l) \delta\left(\pi_{\text{rel}} - \left[\frac{\text{AU}}{D_l} - \frac{\text{AU}}{D_s}\right]\right), \quad (34)$$

where  $D_l$  and  $D_s$  are the lens and source distances. We adopt the Han & Gould (1995, 2003) model, and in Figure 6 we plot  $\pi_{\text{rel}}(M)P[\pi_{\text{rel}}(M)]$  versus  $\log M$  to display the constraint placed on the mass by the measurement of  $\theta_E$ . The full-width half-maximum range is,

$$\log(M/M_\odot) = -0.7 \pm 0.4 \quad (\text{FWHM}). \quad (35)$$

In the absence of such a measurement, the only constraint comes from the measurement of  $t_E$ , and this is extremely weak, having a full width half maximum of a factor  $\sim 100$ . See figure 1 from Gould (2000). Indeed, as shown in that figure, the mere supposition that the lens is a star places stronger constraints on the lens mass than does the measurement of  $t_E$ .

The measurements of  $\theta_E$  and  $t_E$  yield  $\mu_{\text{rel}}$  (eq. [2]). Since the distribution of  $\mu_{\text{rel}}$  varies with  $D_l$  and  $D_s$ , one could in principle use its determination (eq. [32]) to place further constraints on combinations of these parameters and so (through eq. [33]) on the mass. In practice, for bulge sources, the distribution of  $\mu_{\text{rel}}$  hardly varies as a function of lens position, even when one considers bulge versus disk lenses. Moreover, the actual measured value of  $\mu_{\text{rel}}$  is near the peak of that distribution. Hence, we do not incorporate this constraint.

The  $\mu_{\text{rel}}$  measurement does effectively rule out a foreground disk source. (Without this constraint, i.e. from the CMD alone, the source could plausibly be a disk clump giant at  $D_s \sim 5 \text{ kpc}$ ). However, for disk-disk events along this line of sight, the observer, lens, and source all share the same transverse motion due to the flat rotation curve of the Galaxy. Hence, only their peculiar motions relative to this rotation enter  $\mu_{\text{rel}}$ , and these are only of order  $10$ 's of  $\text{km s}^{-1}$ . Hence,  $\mu_{\text{rel}}$  would be only a few  $\text{km s}^{-1} \text{ kpc}^{-1}$ , much slower than the measured value.

The Sumi et al. (2003) proper-motion measurement of the source independently rules out a foreground disk lens, since the source is moving roughly opposite to the direction of Galactic rotation at about  $\mu \sim -v_c/R_0$ , where  $v_c \sim 220 \text{ km s}^{-1}$  and  $R_0 = 8 \text{ kpc}$ . In fact, this measurement by itself would be consistent with the source lying in the background disk, behind the bulge. However, such a scenario is virtually ruled out

by the CMD (see Fig. 2), which shows the source lying in or slightly above the bulge giant branch. If the source lay at, say,  $10 \text{ kpc}$ , it would intrinsically be  $\sim 0.5$  magnitude brighter still.

Combining our measurement  $\mu_{\text{rel}} = 5.6 \text{ mas yr}^{-1}$ , with the Sumi et al. (2003) measurement  $(\mu_\alpha, \mu_\delta) = (-2.9, -12.3) \text{ mas yr}^{-1}$ , we can effectively rule out a disk lens. These measurements imply  $|\mu_L| = |\mu_s + \mu_{\text{rel}}| \gtrsim 7 \text{ mas yr}^{-1}$ , whereas a disk lens would be expected to have roughly zero proper motion.

## 5.2. Lens Luminosity $M_{I,I}$

The measurement of the unlensed background flux,  $F_b$ , gives an upper limit to the flux from the lens. The measured background flux is a function of observatory and filter, and tends to grow with larger mean seeing. Hence, the best constraint is expected to come from the observatory with the best seeing. In our case, this is OGLE. The OGLE  $F_b$  is also by far the best constrained, in part because of the large number of baseline points. The OGLE background-to-source flux ratio is  $F_b/F_s = 0.003 \pm 0.009$ , which yields a  $3\sigma$  lower limit on the magnitude difference of the lens and source,  $I_l - I_s > 3.6$ . For this limit to be at all relevant, the lens must be close to the turnoff or brighter, implying that it is close to a solar mass. Then, from equation (33), the source and lens must be nearly the same distance. This implies in turn that the above limit on apparent-magnitude difference translates directly into a limit on absolute-magnitude difference. Since the source is about 1 mag brighter than the clump, the constraint yields only  $M_{I,I} > 2.4$ , which is of very limited value.

## 6. MICROLENS PARALLAX $\pi_E$

The detection of microlens parallax is marginal. We therefore begin by investigating whether its tentatively detected value is consistent with what else is known about the lens. Given this orientation, and for simplicity of exposition, we ignore the very large error in the measurement. Only one component of the parallax is measured. We therefore actually have a limit, not a measurement, of  $\pi_E \geq |\pi_{E,\parallel}| = 0.86$ . Together with equations (4) and (32), this implies  $M \leq 0.03 M_\odot$  and  $\pi_{\text{rel}} \geq 170 \mu\text{as}$ . The source distance cannot be much more than  $D_s \sim 10 \text{ kpc}$ , partly because of the low density of stars at greater distances and partly because it would lie in an unpopulated portion of the CMD. Hence,  $\pi_l = \pi_{\text{rel}} + \pi_s > 270 \mu\text{as}$ , i.e.  $D_l < 3.7 \text{ kpc}$ . That is, the lens would be a disk brown dwarf.

Apart from the small peculiar velocity of each, the lens and Earth are both rotating about the Galactic center at the same speed. Hence, the lens should be seen moving against the bulge at about  $\sim 220 \text{ km s}^{-1}$  towards Cygnus, which is to say at a position angle roughly  $30^\circ$  east of north. Because the dispersion of bulge stars is about  $90 \text{ km s}^{-1}$ , this should also be approximately the direction of lens motion relative to the source.

Since only one component of  $\pi_E$  is measured, all we can test is the sign of this prediction. From the post-peak residuals to the fit without parallax (Fig. 5), the Earth is accelerating in the direction of the lens motion (thus slowing down the end of the event). On July 19 (roughly one month after opposition), this is basically opposite the direction of the Earth's motion, and so is basically toward the west. Since the field is south of the ecliptic, there is also a small component of this (projected) acceleration toward the south. Hence, the position angle of the projected acceleration vector is about  $260^\circ$ , which is misaligned with the expected direction of the lens



motion by about  $130^\circ$ . That is, the expected sign of  $\pi_{E,\parallel}$  is opposite to what is expected.

While it remains possible that the peculiar velocities of the lens and source conspire to produce this result, the statistical significance of the parallax measurement is not high enough to warrant its acceptance in the face of this strong contrary expectation.

Moreover, there are at least two other possible explanations for this asymmetry apart from statistical fluctuations. The first is xallarap, distortions in the light curve due to accelerated motion of the source rather than the lens. Indeed, Smith, Mao & Paczyński (2003) showed that any parallax effect could be mimicked by the orbital motion of the source around an unseen companion. When both components of  $\pi_E$  are well measured, this possibility can be largely discounted because the probability of the source being in a binary with the same inclination, phase, and period as the Earth's orbit is extremely small. However, in the present case, in which all that is detected is a single component of acceleration, there is a very wide class of source binaries that could mimic the observed parallax signal. Moreover, by the arguments given in § 5.2, any source companion on the main-sequence would be undetectable in the lightcurve (other than through its effect accelerating the source). The xallarap hypothesis could be checked by radial-velocity measurements.

Still another possible source of the asymmetry is a very weak binary lens. Gaudi et al. (2002) detected a similarly weak asymmetry in OGLE-1999-BLG-36 and were able to model this either with parallax or with a low-mass companion to the lens. Thus, asymmetric residuals can be attributed to several effects including parallax, xallarap, and binary lenses.

We thank Martin Smith for valuable comments on the manuscript and Dale Fields for providing us with the best-fit linear limb-darkening coefficients for EROS-BLG-2000-5. Work at OSU was supported by grants AST 02-01266 from the NSF and NAG 5-10678 from NASA. B.S.G. was supported by a Menzel Fellowship from the Harvard College Observatory. C.H. was supported by the Astrophysical Research Center for the Structure and Evolution of the Cosmos (ARCSEC) of Korea Science & Engineering Foundation (KOSEF) through Science Research Program (SRC) program. Partial support to the OGLE project was provided with the NSF grant AST-0204908 and NASA grant NAG5-12212 to B. Paczyński and the Polish KBN grant 2P03D02124 to A. Udalski. A.U., I.S. and K.Ż. also acknowledge support from the grant "Subsydium Profesorskie" of the Foundation for Polish Science.

#### REFERENCES

- Afonso, C., et al. 2000, *ApJ*, 532, 340  
 Albrow, M. D., et al. 1998, *ApJ*, 509, 687  
 Albrow, M. D., et al. 1999a, *ApJ*, 522, 1011  
 Albrow, M. D., et al. 1999b, *ApJ*, 522, 1022  
 Albrow, M. D., et al. 2000a, *ApJ*, 534, 894  
 Albrow, M. D., et al. 2000b, *ApJ*, 535, 176  
 Albrow, M. D., et al. 2001, *ApJ*, 549, 759  
 Alcock, C., et al. 1993, *Nature*, 365, 621  
 Alcock, C., et al. 1995, *ApJ*, 454, L125  
 Alcock, C., et al. 1997, *ApJ*, 491, 436  
 Alcock, C., et al. 2000, *ApJ*, 541, 270  
 Alcock, C., et al. 2001, *Nature*, 414, 617  
 An, J. H., et al. 2002, *ApJ*, 572, 521  
 Aubourg, E., et al. 1993, *Nature*, 365, 623  
 Bessell, M. S., & Brett, J. M. 1988, *PASP*, 100, 1134  
 Bond, I. A., et al. 2001, *MNRAS*, 327, 868  
 DePoy, D. L. et al., 2003, *SPIE*, 4841, 827  
 Dominik, M. 1998, *A&A*, 333, 893  
 Eisenhauer, F., Schoedel, R., Genzel, R., Ott, T., Tecza, M., Abuter, R., Eckart, A., & Alexander, T. 2003, *ApJL*, submitted (astro-ph/0306220)  
 Fields, D. L., et al. 2003, *ApJ*, in press.  
 Gaudi, B. S., et al. 2002, *ApJ*, 566, 463  
 Gould, A. 1992, *ApJ*, 392, 442  
 Gould, A. 1994a, *ApJ*, 421, L71  
 Gould, A. 1994b, *ApJ*, 421, L75  
 Gould, A. 1995, *ApJ*, 441, L21  
 Gould, A. 2000, *ApJ*, 535, 928  
 Gould, A. & Loeb, A., *ApJ*, 396, 104  
 Gould, A., Miralda-Escudé, J., & Bahcall, J.N. 1994, *ApJ*, 423, L105  
 Gould, A. & Welch, D.L. 1995, *ApJ*, 464, 212  
 Gradshteyn, I. S., & Ryzhik, I. M. 1965, *Table of Integrals Series and Products* (London: Academic Press)  
 Griest, K. & Safizadeh, N. 1998, *ApJ*, 500, 37  
 Han, C., & Gould, A. 1995, *ApJ*, 447, 53  
 Han, C., & Gould, A. 2003, *ApJ*, 592, 172  
 Nemiroff, R. J., & Wickramasinghe, W. A. D. T. 1994, *ApJ*, 424, L21  
 Paczyński, B. 1986, *ApJ*, 304, 1  
 Paczyński, B. 1996, *Acta Astron.*, 48, 405  
 Paczyński, B., & Stanek, K.Z. 1998, *ApJ*, 494, L219  
 Popowski, P. 2000, *ApJ*, 528, L9  
 Press, W. H., Flannery, B. P., Teukolsky, S. A., & Vetterling, W. T. 1992, *Numerical Recipes* (Cambridge: Cambridge Univ. Press)  
 Refsdal, S. 1966, *MNRAS*, 134, 315  
 Rhie, S. H., Becker, A. C., Bennett, D. P., Fragile, P. C., Johnson, B. R., King, L. J., Peterson, B. A., & Quinn, J. 1999, *ApJ*, 522, 1037  
 Salim, S., & Gould, A. 1999, *ApJ*, 523, 633  
 Schechter, P. L., Mateo, M., & Saha, A. 1993, *PASP*, 105, 1342  
 Smith, M. C., Mao, S., & Paczynski, B. 2003, *MNRAS*, 339, 925  
 Smith, M. C., Mao, S., & Woźniak, P. 2003, *ApJ*, 585, L65  
 Stutz, A., Popowski, P., & Gould, A. 1999, *ApJ*, 521, 206  
 Sumi, T., et al. 2003, *MNRAS*, submitted (astro-ph/0305315)  
 Udalski, A., et al. 1993, *Acta Astron.*, 43, 289  
 Udalski, A., Szymański, M., Kałużny, J., Kubiak, M., Mateo, M., Krzemiński, W., & Paczyński, B. 1994, *Acta Astron.*, 44, 227  
 Udalski, A., et al. 2000, *Acta Astron.*, 50, 1  
 Udalski, A. 2003, *ApJ*, 590, 284  
 Udalski, A., et al. 2002a, *Acta Astron.*, 52, 1  
 Udalski, A., et al. 2002b, *Acta Astron.*, 52, 217  
 van Belle, G. T. 1999, *PASP*, 111, 1515  
 Witt, H. J., & Mao, S. 1994, *ApJ*, 430, 505  
 Woźniak, P. R. 2000, *Acta Astron.*, 50, 421